A characterization and modeling of the gravity-driven flashing of superheated water in a pool heated from below

Jimmy Martin,[*,a,b] Pierre Ruyer,[a] Matthieu Duponcheel,[b] and Yann Bartosiewicz[b]

[a] *Institut de Radioprotection et de Sûreté Nucléaire (IRSN)*
Saint-Paul-lez-Durance, 13115, France

[b] *UCLouvain, Institute of Mechanics, Materials and Civil engineering*
Louvain-la-Neuve, B-1348, Belgium

[*]Email: jimmy.martin@irsn.fr

Number of pages: 33
Number of tables: 2
Number of figures: 21

Abstract

The gravity-driven flashing of superheated water, topic of the present paper, is a phase change phenomenon which is tightly linked with some of the safety issues of the spent-fuel-pool loss-of-cooling accident. As detailed in this article, the phenomenon has been empirically studied and characterized within the so-called Aquarius laboratory-scale experimental device. Primarily, the performed tests unveil the occurrence conditions of the gravity-driven flashing phenomenon in a pool heated from below and its coupling with the degassing of dissolved gases that may take place within the liquid. Next, a set of dimensionless correlations describing the studied heat and mass transfers is derived from the data and presented, both for the single and two-phase regimes of any conducted test. Then, a lumped-parameter model, relying on those correlations and describing the studied physics is introduced. The model resolves the coupled mass and energy balance equations of the heated liquid pool. At last, this model is used for simulating a selected reference test. The performed simulations are successfully compared with the available empirical data, with moderate discrepancies, thereby verifying the adequateness of the proposed model.

Keywords — spent-fuel-pool, loss-of-cooling accident, heat and mass transfer correlations, lumped-parameter model

I. INTRODUCTION

The March 11, 2011 Fukushima-Daiichi nuclear power station accident has emphasized the vulnerability of spent-fuel-pools (SFP), a type of nuclear system whose accidentology has been only poorly studied during the past decades. For assessing the level of knowledge associated with SFPs, two international working groups were set up following the Fukushima-Daiichi accident, under the auspices of the *Nuclear Energy Agency* (NEA) of the *Organisation for Economic Cooperation and Development* (OECD). At first, a so-called *Status Report* on SFPs has been published in 2014. This report summarizes what was known on SFP accidents to date and reviews the several SFP designs that can be met worldwide, the possible accident mitigation strategies and the availability of SFP simulation tools and experimental data [1]. Later, a phenomena identification and ranking activity was performed at OECD/NEA on that very topic and shared with the community in 2018 [2], [3]. Among the phenomena that have been identified on this occasion is the gravity-driven flashing of superheated water, discussed in the present article.

First of all, the phenomenon is expected to occur in any system where an uprising fluid, heated from below, experiences a significant decrease in hydrostatic pressure. In doing so, the uprising liquid temperature may potentially exceed its saturation value, bringing the fluid into its metastable domain. As a way to relax toward thermal saturation, the superheated liquid may then spontaneously vaporize through the form of bubbles, a process referred to as *flashing* [4]. Especially, this relaxation process concentrates most of the uncertainties related to the phenomenon. Indeed, as any bubble nucleation process, the spontaneous flashing of superheated water may depend on many extraneous factors such as the presence within the liquid of solid impurities, dissolved gases, chemical surfactants [5], or water molecules ionized by an incoming subatomic particle, [6], [7]. For obvious reasons, those molecular-scale or subatomic factors are often if not always difficult to characterize, making uncertain the mechanisms by which the superheated liquid may relax [8].

Because of their typical depth of the order of 10 m yielding a vertical difference in water saturation temperature around 20°C and a significant amount of dissolved air within their liquid volume, SFPs have been early recognized as industrial systems where the phenomenon might be observed under accidental conditions [1], as idealized in Figure 1. Nevertheless, in spite of some significant studies of the phenomenon in vertical pipes or ducts heated from below, *e.g.* [9] or [10], or in the unheated pool of a flash evaporator, *e.g.* [11], [12] or [13], the specific configuration of a

pool heated from below had not been studied yet at the time of Fukushima-Daiichi accident [14]. But possibly, if the phenomenon were to occur in the course of such accident, the resulting bubble production would prevent any restarting of the SFP cooling system and would contribute to the release of numerous residual radionuclides normally contained in water [2], [15], well before the spent nuclear fuels get uncovered.

Owing to the potentially harmful consequences of the phenomenon and the lack of experimental evidence regarding its existence in pools heated from below, a specific research program has been launch at the French *Institut de Radioprotection et de Sûreté Nucléaire* (IRSN) [16]. In this framework, an integral experimental facility named *MIDI* reproducing at a small scale the thermal-hydraulics of a SFP loss-of-cooling accident has been constructed and has yielded a first series of results [17], [18]. Overall, it has been shown that the phenomenology, reproduced at the integral scale of the MIDI facility, mostly complies with the one that was envisioned by the community right after the Fukushima-Daiichi nuclear accident. However, in spite of these promising results, there is still a need to separately study the gravity-driven flashing in a pool heated from below, by means of an analytical experiment. In order to fulfil this need, the IRSN's research program also comprises a collaboration with the *Université catholique de Louvain* (UCLouvain, Belgium) that has been initiated in 2018 on that topic. In this context, a 1:25-scale simplified SFP mock-up named *Aquarius* has been designed and built-up with the intent to investigate the phenomenon (*cf.* Figure 2). The retained downscaling method mainly consists in an operating pressure distortion, which allows conserving a large saturation temperature vertical difference even at a reduced scale, with an appropriate choice of system's pressure (see [19] for more details). Indeed, in the low-pressure case, because of existing steep variations in saturation temperature against pressure, a little variation in hydrostatic pressure, provided by a reduced pool level, may be enough for achieving some required large vertical saturation temperature difference [19]. Later on, an extensive experimental campaign has been conducted and its first results have been shared with the community, successively in [14], [20] and [21]. The present paper goes beyond those early reports by providing the reader with a first characterization of the heat and mass transfers developing at pool scale during a typical Aquarius test and with a simplified modeling of the studied phenomenon.

Thus, after providing in Section II a brief description of the Aquarius test device and in

Section III.A, an overview of the experimental results obtained to date, the heat and mass transfers associated with the phenomenon are quantified in Section III.B. Next, the repeatability of the obtained results is discussed in details in Section III.C. Then, a so-called lumped-parameter modeling of the heated pool is introduced in Section IV. At last, the model is used for simulating a so-called reference test in Section V, which allows assessing its predictability with regards to the studied physics.

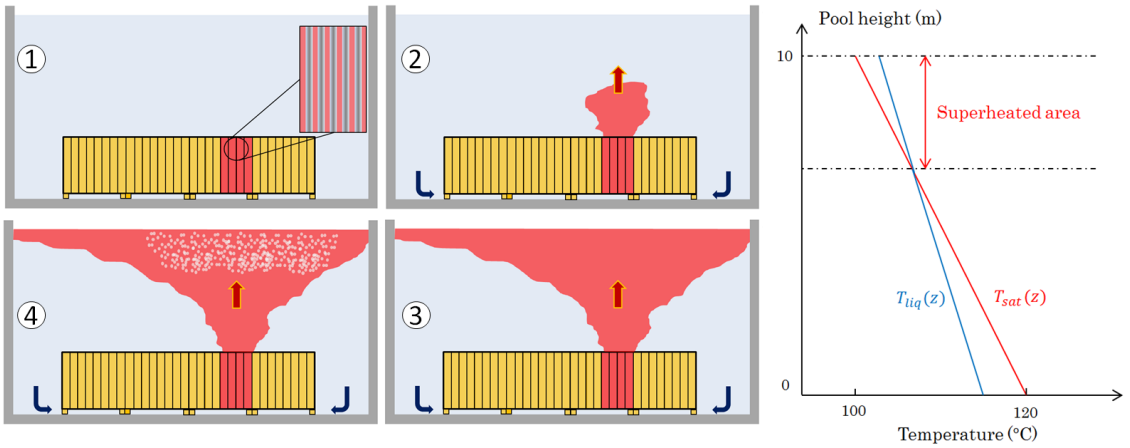

Fig. 1. The gravity-driven flashing in a spent-fuel-pool. Left-hand-side: 1) Water is heated up by the spent fuels and keeps subcooled, 2) A natural convection flow develops at pool scale, 3) The saturation temperature is locally exceeded in the upper part of the pool by the uprising water, 4) The superheated water flashes and turns into bubbles. Right-hand-side: idealized vertical profile of the water temperature and of the boiling point within the uprising plume [19].

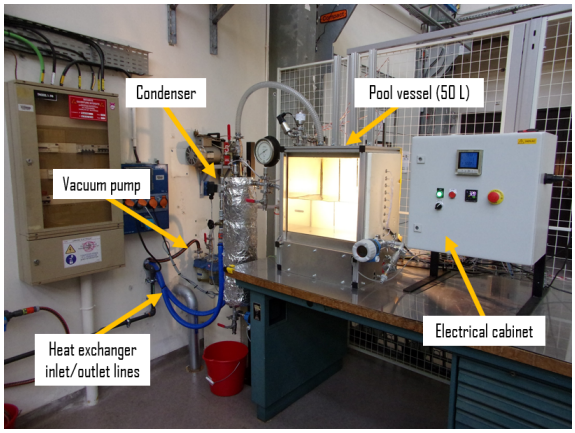

Fig. 2. Overview of the Aquarius test device designed and operated by IRSN / UCLouvain for investigating the gravity-driven pool flashing phenomenon at a laboratory scale [19].

II. THE EXPERIMENTAL DEVICE

II.A. Characteristics

The experimental device, illustrated in Figure 3, consists in a 54 L closed vessel of height $H = 40$ cm, length $L = 45$ cm and width $W = 30$ cm. The vessel is connected to a vacuum pump and a condenser. The vacuum pump allows imposing low pressure conditions down to 10 mbar within the gaseous upper volume of the vessel. Once those conditions are reached, the condenser keeps a constant pressure within this latter volume. As visible in Figure 4, working under those low pressure conditions yields a large vertical variation in the water saturation temperature at the scale of the test device, of the order of 20°C, thereby allowing a liquid heating at the bottom of the pool without boiling, as expected during a SFP loss-of-cooling accident. On that basis, it can be envisioned to reach metastability conditions in the upper part of the pool, as the liquid rises by natural convection, and a subsequent phase change. A planar heating element, providing a 1-kW maximum thermal power to the water pool is placed at the bottom of the vessel. It is worth pointing out that this element is geometrically simplified with respect to a real SFP heat source. Its area represents 75% of the bottom surface. This electrically operated device is split into two separate parts, thereby allowing a spatially heterogeneous heating of the water. Two parallel optical windows allow observing the phenomenon (see Figure 2). All other immersed surfaces are made of stainless steel.

II.B. Instrumentation

The device is equipped with four Pt-100 class A temperature probes whose position can be manually modified within the liquid bulk or its sky and with twelve Pt-100 probes embedded in one of the lateral walls of the vessel and in the heaters. Two pressure sensors are located on top of the vessel for monitoring its boundary pressure with two complementing accuracy levels. One sensor is installed at its bottom-end, in order to catch liquid mass variations throughout the tests. In addition, aware of the importance of dissolved gases for the studied phenomenon [5], an optical dissolved oxygen sensor (Hamilton VisiFerm™DO Arc 120) measures continuously the amount of oxygen within water. A FASTCAM™SA3 model 120K-M1 high-speed camera is occasionally placed in front of one of the two optical windows. The condenser, illustrated in Figure

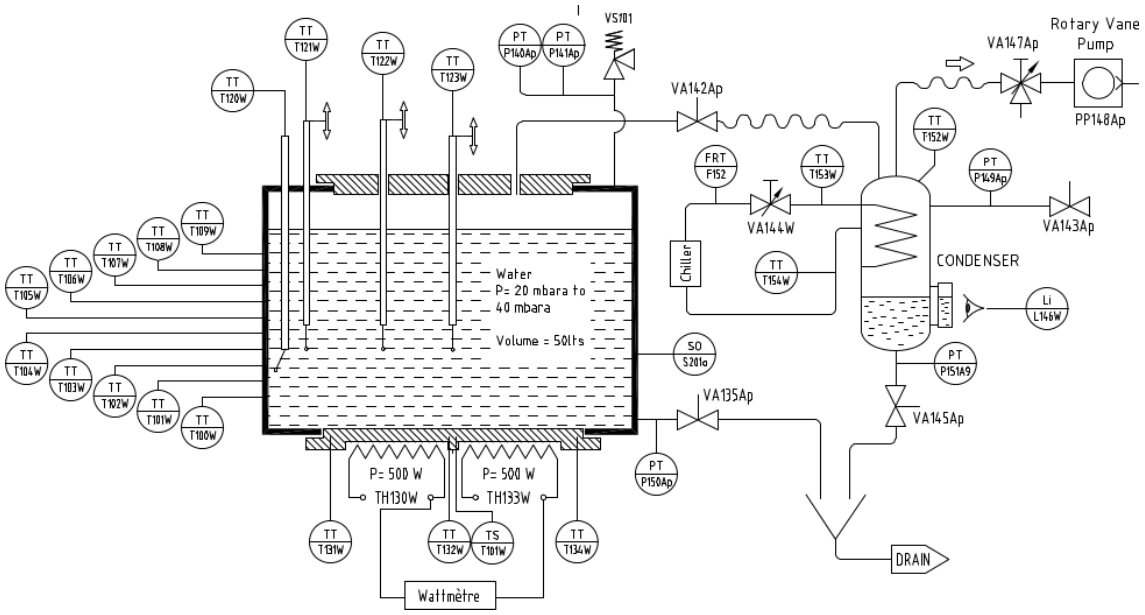

Fig. 3. Piping and instrumentation diagram of the experimental device.

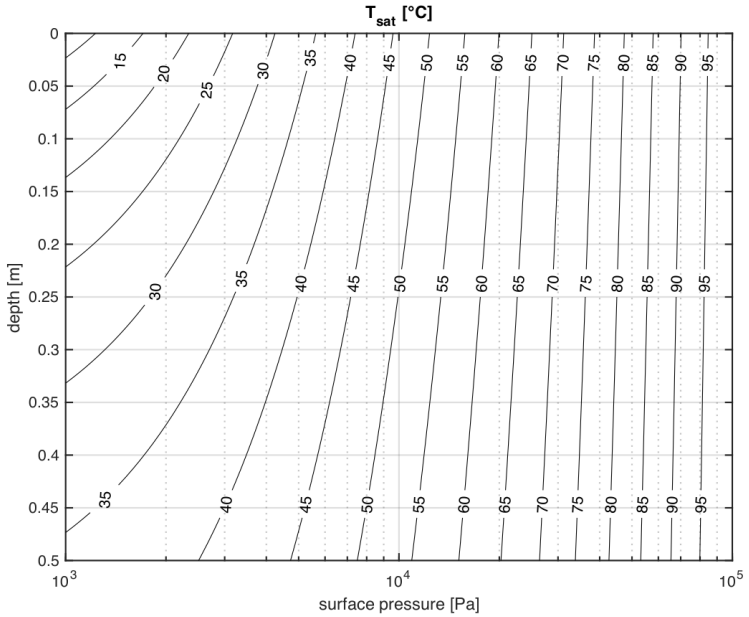

Fig. 4. Vertical variation of the water saturation temperature in the liquid pool against the operating pressure, imposed at the liquid free surface. As one can notice, the lower the operating pressure, the bigger the vertical variation in saturation temperature.

3, is also instrumented in order to control and monitor the test conditions. It is equipped with two pressure sensors. One is located at its bottom-end and follows changes in its liquid inventory. One is installed at its top-end, in its gaseous volume, together with a temperature measurement. Two more temperature sensors are located at the inlet and outlet sections of the heat exchanger which is embedded within the condenser. At last, a flow-meter provides the water mass flow rate circulating through the heat exchanger (*cf.* [19] for more details).

II.C. Measurement uncertainties

As it will be seen later in this article, a limited set of physical variables does appear relevant for characterizing the performed experiments. Those variables, further introduced in Section III, are:

- ΔT_{eq}: the so-called liquid thermal metastability degree;
- P_G: the vessel's operating pressure;
- m_L: the liquid pool mass;
- $\dot{m}_L$: the liquid vaporization rate;
- C_{O_2}: the dissolved O_2 concentration;
- $\dot{C}_{O_2}$: the O_2 degassing rate;
- $k_T^L S_i$: the heat transfer rate;
- $k_m^L S_i$: the mass transfer rate associated with the air degassing.

The uncertainties in link with the latter variables were all estimated according to a methodology which complies with the recommendations of the *Guide to the expression of uncertainty in measurement* - or GUM - a reference guideline in metrology [22], as detailed in [19]. The approach, taking benefit from a set of repeatability tests (*cf.* Section III.C), yielded the results given in Table I, with a retained coverage factor of 95%. At last, it is to be noted that the magnitude of the error bars illustrated in the following graphs is obviously based on the data given in Table I.

TABLE I
Combined uncertainties with a coverage factor of 95%.

Parameter	**Combined uncertainty (coverage factor: 95%)**
Liquid thermal metastability degree ΔT_{eq}	0.4°C
Vessel's atmosphere pressure P_G	5.5%
Liquid pool mass m_L	0.74 kg
Liquid vaporization rate $\dot{m}_L$	0.10 g/s
Dissolved O_2 *concentration* C_{O_2}	3.9%
O_2 *degassing rate* $\dot{C}_{O_2}$	6.1%
Heat transfer rate $k_T^L S_i$	19%
Mass transfer rate $k_m^L S_i$	19%

II.D. Experimental procedure

The pool flashing experiments presented in this article were all achieved according to the following test procedure:

- **Filling stage**: the pool is filled up or partially drained, depending on the required initial water level;
- **Bubbling stage**: the liquid pool is bubbled by means of the laboratory compressed air system, in order to reach a targeted and measured initial content in dissolved O_2 (if required);
- **Chiller start-up**: the chiller is parametrized and started-up, in order to reach a stationary cold source temperature prior to the test;
- **Heaters start-up**: the required heat power is fixed by means of a rheostat and the heaters are then electrically fed, which leads to a progressive increase of the liquid temperature, denoted as T_L, up to its targeted value;
- **Depressurization**: once the required initial pool temperature is reached, the depressurization is initiated by starting up the vacuum pump. The vessel pressure naturally tends towards $P_{sat}(T_L)$, *i.e.* the saturation pressure corresponding to the initial liquid pool temperature T_L. At that stage, the pool atmospheric volume is quasi-exclusively filled with steam water and hence highly depleted in air (however, the liquid still contains some dissolved gases);
- **Pressure regulation**: the vacuum pump is kept working throughout the test and the condenser heat exchanger valve is regulated by the operator (the cold source temperature set

point being kept unchanged), both operations allowing the pool pressure to remain stable along the vaporization and degassing processes.

This procedure systematically initiates a pool flashing test at thermal saturation conditions, *i.e.* $T_L(t=0) = T_{sat}(P_G)$.

III. AN OVERVIEW OF THE OBTAINED EXPERIMENTAL RESULTS

III.A. The overall phenomenology

In what follows, we first provide the reader with some key features of the studied physics that are presented in more details in [19]. The observations that are discussed next are based on a typical test conducted with a thermal power $\dot{Q}_p = 1$ kW, an operating pressure imposed at the liquid free surface P_G of 22 mbar, an initial pool level z_p of 30 cm and an initial content in dissolved oxygen $C_{O_2} = 5.8$ mg/L (value in excess at a pressure of 22 mbar). At first, during the considered experiment, by launching the test under thermal saturation conditions the liquid rapidly started to vaporize at a constant rate, as visible in Figure 5. Throughout the test, the gas volume located on top of the liquid free surface remained fully filled with steam at a temperature $T_G \approx T_{sat}(P_G)$.

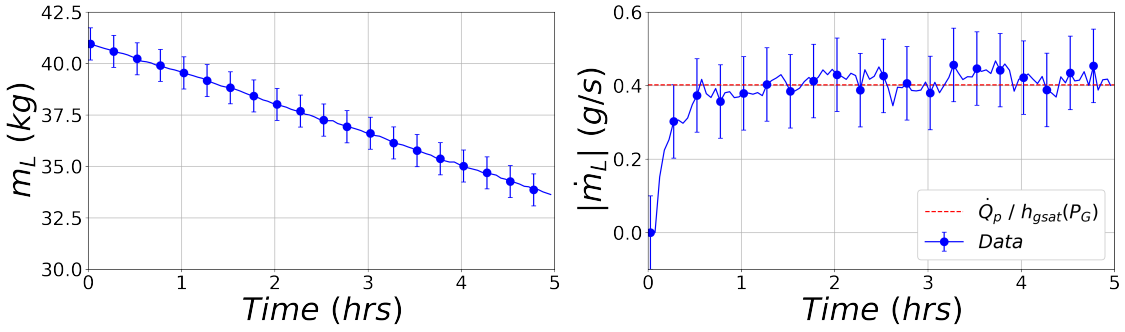

Fig. 5. Reference test. Left: liquid mass m_L, estimated from an hydrostatic pressure difference measurement. Right: estimated liquid vaporization rate $\dot{m}_L$.

However, in spite of the noticed steady liquid vaporization, the liquid pool evolved thermodynamically according to a two-stage process which is the direct consequence of the imposed initial excess in dissolved gases [21]. During the first stage, referred to as *two-phase regime* and which lasted approximately 45 min, a strong and continuous bubbling due to the flashing of some metastable liquid was observed below the water free surface, as represented in Figure 6. This latter

process gradually weakened over time, yielding fewer but bigger bubbles. Then, after about 45 min, a second regime settled. This stage, characterized by a lack of any sustained bubble nucleation as noticeable in Figure 7, is later referred to as *single-phase regime*. At that very stage, most of the water vaporization was supported by the only free surface evaporation. Importantly, one has to note that when starting a test with an initial dissolved O_2 mass concentration below an estimated threshold value of 0.7 mg/L, this single-phase regime was directly and systematically reached from the very beginning of the test and no sustained bubble nucleation was observed at all [21]. Thus, this observation clearly highlights the key role played by the gases initially in solution within the liquid during its gravity-driven flashing [20].

Fig. 6. Overview of the Aquarius pool with a flashing of the superheated water taking place exclusively below the liquid free surface (notice the presence of numerous bubbles at that location).

In the first reports of this phenomenology done in [14] and [20], two quantities have been proven important for describing the phenomenon: the so-called *liquid thermal metastability degree* ΔT_{eq} and the measured dissolved O_2 mass concentration, denoted as C_{O_2}, which gives an estimate of the instant amount of air in solution within the water pool (indeed, the N_2 concentration may be inferred from the O_2 concentration measurement, as justified in [19]). As firstly discussed in [14], all measured liquid pool temperatures significantly deviated over time from the saturation temperature $T_{sat}(P_G)$, corresponding to the pool's initial state. Obviously, this reveals that the liquid, initially at thermodynamic stable equilibrium (*i.e.* at thermal saturation) entered more and more into its metastable domain as time went by. It is interesting to determine up to which metastable state the liquid evolved. For doing so, the variable ΔT_{eq} has been introduced. It is

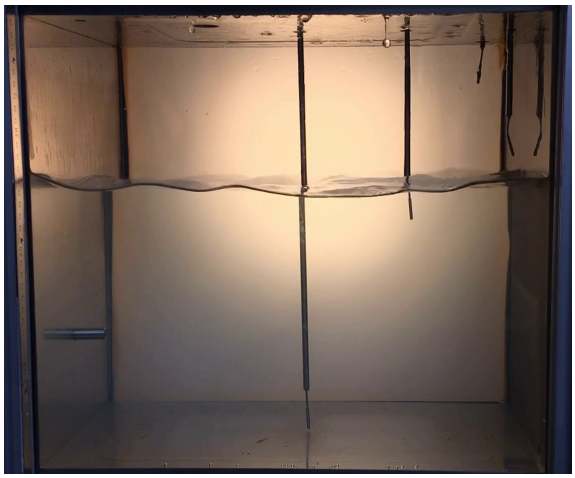

Fig. 7. The late single-phase regime of any gravity-driven pool flashing test conducted by means of the Aquarius device (notice the absence of any bubble). This regime is typically reached when the amount of dissolved oxygen is below an approximate threshold value of 0.7 mg/L.

defined as:

$$\Delta T_{eq} = < T_L > - T_{sat}(P_G) \tag{1}$$

with $< T_L >$ the arithmetic mean of the measured liquid bulk temperatures. The application of Equation (1) to the presented test data is illustrated in Figure 8. One can observe that the liquid metastability degree did not increase indefinitely during the test. Indeed, it appears that from t = 3 hrs, ΔT_{eq} stabilized at an approximate value of 4.5°C, denoted as $\Delta T_{eq;\infty}$, up to the end of the test. Pointedly, this so-called *asymptotic state* of the metastable liquid maintained during a relatively long period of 2 hrs, in spite of some noticeable sporadic but violent events of bubble nucleation [21].

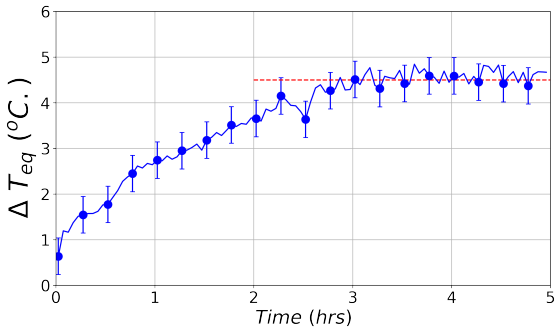

Fig. 8. Estimate of the thermal metastability degree of the heated liquid ΔT_{eq} during the presented test. From $t = 3$ hrs, ΔT_{eq} stabilized at a value of 4.5°C, up to the end of the test.

Let us then study the time-variations of the amount of dissolved gases in the liquid pool. For that purpose, the left-hand-side graph of Figure 9 represents the direct measurement of the dissolved oxygen concentration within the liquid. The right-hand-side graph of this very figure is an estimate of the O_2 degassing rate, denoted as $\dot{C}_{O_2}$. One can observe that, as expected, the dissolved O_2 concentration, initially in excess, decreased over time as a system's way for reaching a chemical equilibrium state with regards to this very species. Then, it is worth pointing out that the O_2 degassing flux, which was almost null initially, peaked temporarily at a value of approximately 17 mg/L/s, before dropping back to low values, from $t = 60$ min. This suggests the existence of a substantial dissolved O_2 mass transfer within the liquid pool, during the initial two-phase regime of the test. To conclude, it is interesting to notice that the time-variations of ΔT_{eq} and C_{O_2} were correlated, as seen in Figure 10. This graph exhibits two linear trends, which intersect at $C_{O_2} \approx 0.55$ mg/L for the presented test. Finding from Figure 9 the time corresponding to the reach of $C_{O_2} = 0.55$ mg/L yields approximately 45 min, *i.e.* more or less the observed duration for the bubbling regime. This clear and abrupt change in the two linear trends slope is hence interpreted as reflecting the transition between the bubbling/non-bubbling regimes that was evidenced above.

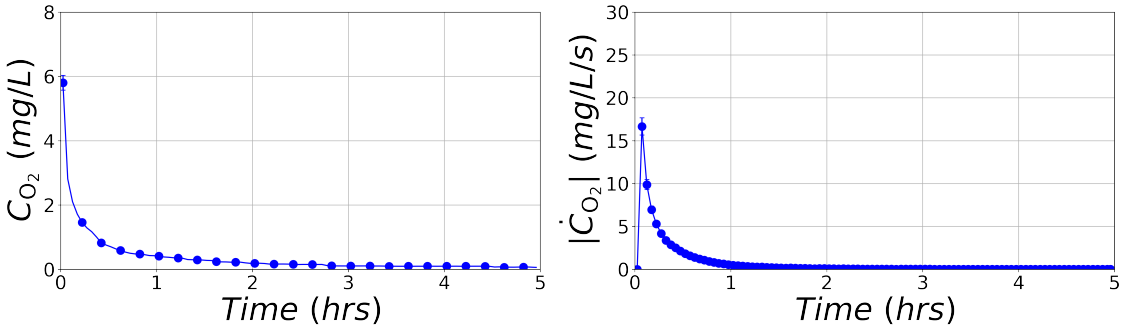

Fig. 9. Reference test. Left: measured dissolved oxygen concentration C_{O_2}. Right: estimated oxygen degassing rate $\dot{C}_{O_2}$.

III.B. The typical time-trend of the gas/liquid interfacial heat and mass transfers

From the presented data, one can derive the gas/liquid interfacial heat and mass transfer rates, respectively denoted as $k_T^L S_i$ and $k_m^L S_i$, that are illustrated in Figure 11. Firstly, if one assumes that the main part of the gas/liquid heat transfer takes place in the vicinity of the liquid free surface (indeed, the bubbles mostly grow underneath the liquid free surface, as seen in Figure

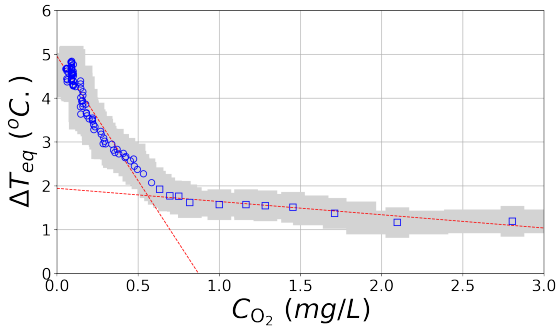

Fig. 10. Reference test. The variables reflecting the liquid degassing and heat-up kinetics, C_{O_2} and ΔT_{eq}, were linearly correlated according to a pair of trends that intersected at a time estimated to 45 min, in consistency with the visualized transition between a two-phase regime and a single-phase regime.

6), one can model the liquid vaporization process by the following heat fluxes continuity equation:

$$k_T^L S_i \Delta T_{eq} = |\dot{m}_L| \mathcal{L}_w \tag{2}$$

with k_T^L, the gas/liquid heat transfer coefficient given in W/m^2/K, S_i the gas/liquid interfacial area, ΔT_{eq} the already introduced liquid metastability degree, $\dot{m}_L$ the liquid vaporization rate and $\mathcal{L}_w$ the water latent heat. In Equation (2), both k_T^L and S_i are unknown in the general case and must be resolved jointly. Interestingly, S_i is doubtless equal to S_p, the liquid free surface area, in the single-phase regime of any experiment, thereby allowing a direct estimate of k_T^L only in this very case. In what follows, an emphasis will be put on the product $k_T^L S_i$, specifically referred to as the gas/liquid heat transfer rate. In a similar way for the mass transfer rate, let us denote as k_m^L the dissolved air mass transfer coefficient, given in kg/m^2/s, characterizing the overall degassing process of O_2 and N_2 species, depicted in Figure 11. With both O_2 and N_2 being largely diluted in water, this mass transfer coefficient can be related to the instant mass flux of dissolved air $\dot{m}_a^L$, given in kg/s, by means of the following simple linear relation [23]:

$$\dot{m}_a^L = - \underbrace{k_m^L S_p (\omega_a^L - \omega_a^{Li})}_{\text{transfer through free surface}} \underbrace{- k_m^L (S_i - S_p)(\omega_a^L - \omega_a^{Bi})}_{\text{transfer through bubbles}} \tag{3}$$

with ω_a^L the mass fraction of dissolved air, constant anywhere in water and equal to:

$$\omega_a^L = \frac{C_a}{\rho_L} \tag{4}$$

where $C_a \approx C_{O_2}/0.34$ is the dissolved air mass concentration (see [19] for more details about the equivalence between the dissolved air and dissolved O_2 mass concentrations) and ρ_L, the liquid density. Further, ω_a^{Li} is the equilibrium value of ω_a^L, supposedly reached at the liquid free surface and ω_a^{Bi}, its counterpart at the bubbles interface. With an air partial pressure P_a^G in the vessel's gas volume being approximately null throughout the studied experiments (*cf.* Section III.A), then C_a^{Li} and consequently $\omega_a^{Li} \approx 0$ according to the so-called Henry's law of gas solubility. Moreover, as it has been evidenced in [19], the liquid vaporization process completely dominates the bubble growth that is observed during any typical experiment. Under this condition, one can reasonably assume that the gas content of the observed bubbles is mainly constituted by steam, yielding too $P_a^B \approx 0$, the partial pressure of air inside the bubbles and then at the liquid side $\omega_a^{Bi} \approx 0$, according to Henry's law. Hence:

$$\dot{m}_a^L \approx -k_m^L S_i \frac{C_a}{\rho_L} \tag{5}$$

In this equation, $\dot{m}_a^L$ can be replaced by the time-derivative of $C_a \approx C_{O_2}/0.34$, which is a measured quantity. Noticing that:

$$m_a^L = C_a V_L \tag{6}$$

with V_L the liquid water volume, one gets:

$$\dot{m}_a^L = C_a \dot{V}_L + V_L \dot{C}_a \tag{7}$$

In addition, with:

$$V_L = \frac{m_L}{\rho_L} \tag{8}$$

then:

$$\dot{V}_L = \frac{1}{\rho_L}\dot{m}_L - \frac{m_L}{\rho_L^2}\dot{\rho}_L \tag{9}$$

Next, one can approximate $\dot{\rho}_L$ as [24]:

$$\dot{\rho}_L = -\rho_L \beta_L \dot{T}_L \tag{10}$$

with β_L, the so-called liquid isobaric expansion coefficient, which yields:

$$\dot{m}_a^L = C_a \left(\frac{1}{\rho_L} \dot{m}_L + \frac{m_L}{\rho_L} \beta_L \dot{T}_L \right) + V_L \dot{C}_a \tag{11}$$

Then, inserting Equation (5) into (11) with $\dot{C}_{O_2}/C_{O_2} \approx \dot{C}_a/C_a$ (*cf.* [19] for a complete demonstration), one gets:

$$k_m^L S_i = -\left(\dot{m}_L + m_L \beta_L \dot{T}_L + \frac{m_L}{C_{O_2}} \dot{C}_{O_2} \right) \tag{12}$$

At last, the application of Equations (2) and (12) to the empirical data of the presented test is exhibited in Figure 12. It is interesting to notice that $k_T^L S_i$ was maximum during the strong bubbling stage highlighted above and visible in Figure 6. Starting from high initial values, $k_T^L S_i$ decreased gradually toward an asymptotic value, denoted as $(k_T^L S_i)_\infty$ and equal to 230 W/K. The same observation may be consistently done for $k_m^L S_i$, as seen in the right-hand-side of Figure 12.

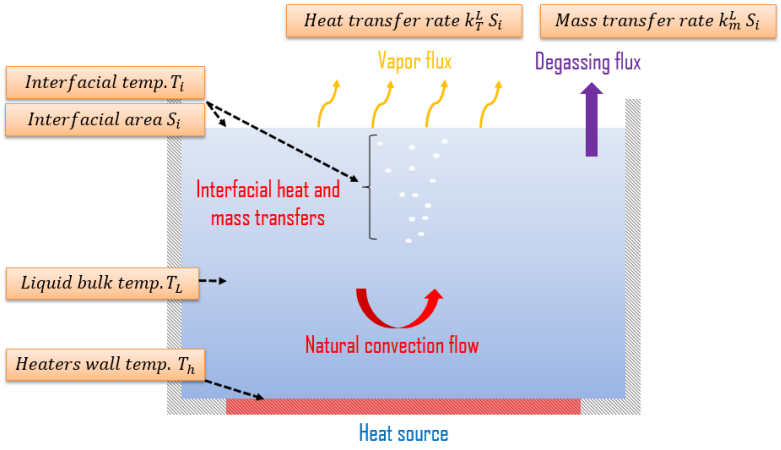

Fig. 11. An idealization of the heat and mass transfers taking place between the liquid bulk and the overall gas/liquid interfacial area (all bubbles + pool free surface), during the two-phase regime.

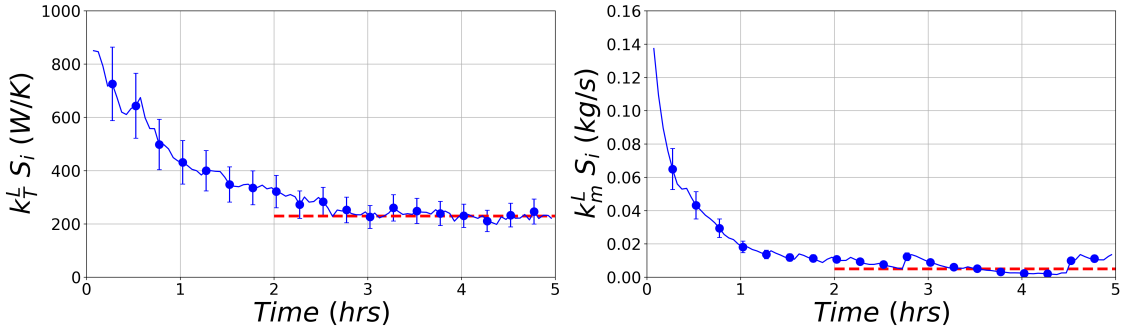

Fig. 12. Reference test. Left: estimate of the gas/liquid heat transfer rate $k_T^L S_i$. Right: estimate of the gas/liquid mass transfer rate $k_m^L S_i$. The unresolved initial value of those transfer rates is intentionally missing.

III.C. A repeatable phenomenology

Next, it is worth verifying the repeatability of the overall phenomenology that is discussed in Section III.A. In order to do so, we analyse in what follows the results obtained during nine identical tests, whose settings were as close as possible to those of the so-called reference test. A comparison of the most relevant physical quantities characterizing these tests is first provided in Figure 13. In the latter figure, one can notice the overall good repeatability of those physical variables. Indeed, the observed time trends were all repeatable, with a relatively small level of discrepancy from one test to another. The calculated time-averaged standard deviations, associated with the differences in each variable X value from test to test, are referred to as $\bar{\sigma}_X$. They are further given in Table II.

TABLE II
Calculated time-averaged standard deviations associated with each main physical variable, on the basis of the nine repeated tests.

Parameter	Time-averaged standard deviation	Value
Liquid thermal metastability degree	$\bar{\sigma}_{\Delta T_{eq}}$	0.17°C
Vessel's atmosphere pressure	$\bar{\sigma}_{P_G}$	0.53 mbar
Liquid pool mass	$\bar{\sigma}_{m_L}$	0.32 kg
Liquid vaporization rate	$\bar{\sigma}_{\dot{m}_L}$	0.03 g/s
Dissolved O_2 concentration	$\bar{\sigma}_{C_{O_2}}$	0.09 mg/L
O_2 degassing rate	$\bar{\sigma}_{\dot{C}_{O_2}}$	0.19 mg/L/s

Obviously, with such a good repeatability of the computed ΔT_{eq} and measured C_{O_2}, the cor-

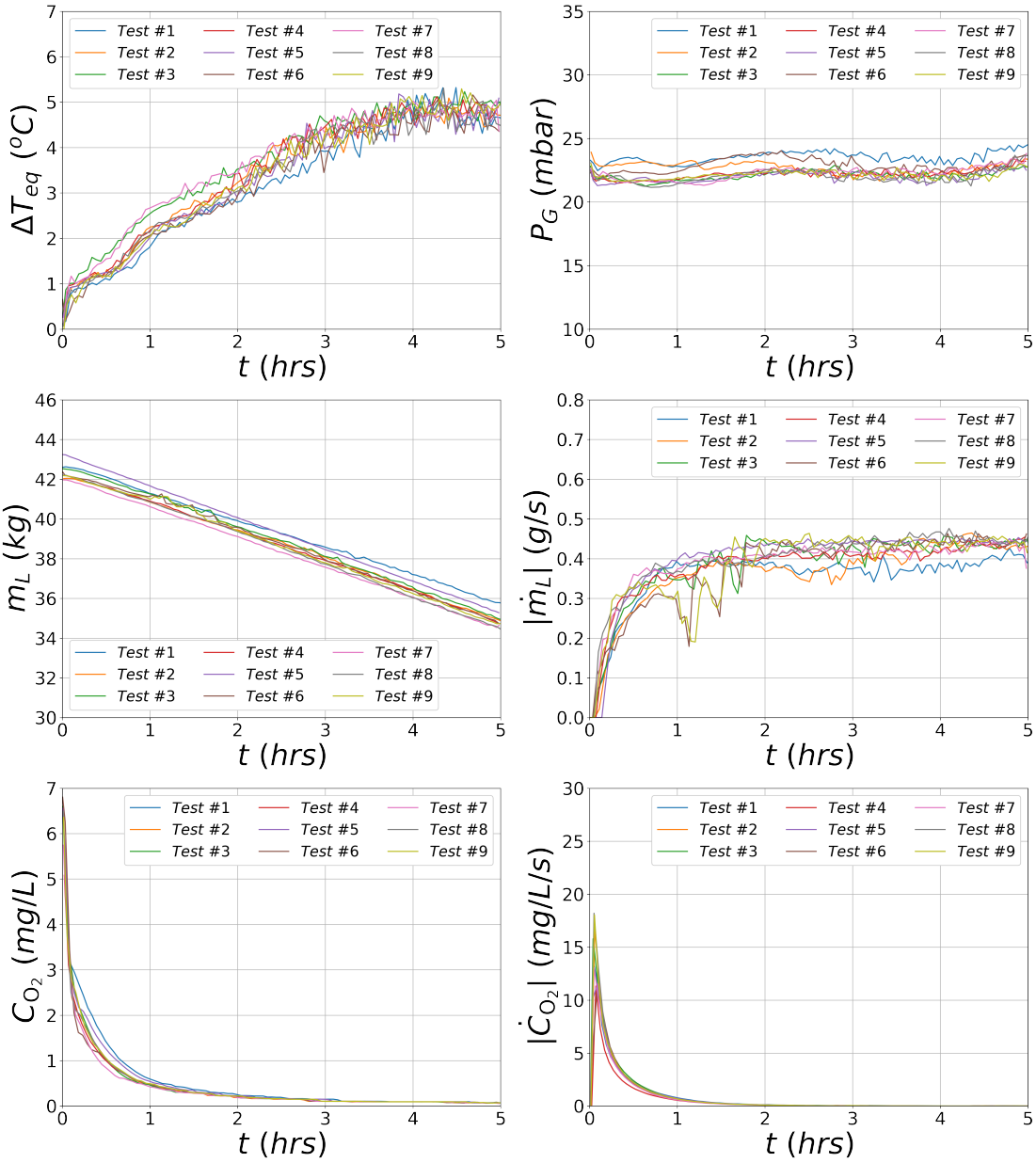

Fig. 13. The main physical variables of the achieved nine identical tests, having parameters as close as possible to those of the so-called reference test. One can notice the overall good repeatability of the considered physical quantities.

relation that has been found between the latter two variables in Section III.A is to be repeatable as well. This is indeed verified in Figure 14. The C_{O_2} threshold value, postulated as reflecting the transition between the bubbling/non-bubbling regimes and equal to 0.55 mg/L for the reference test, is actually much closer to 0.45 mg/L when considering more data points. The overall

phenomenology, described in Section III.A, was also repeatable with some insignificant slight discrepancies detailed in [19]. Whatever the repeated test, a bubbling regime similar to the one visible in Figure 6 invariably lasted around 45 min. It was then systematically followed by a single-phase regime, revealed by the absence of any sustained bubble nucleation process, as noticeable in Figure 7.

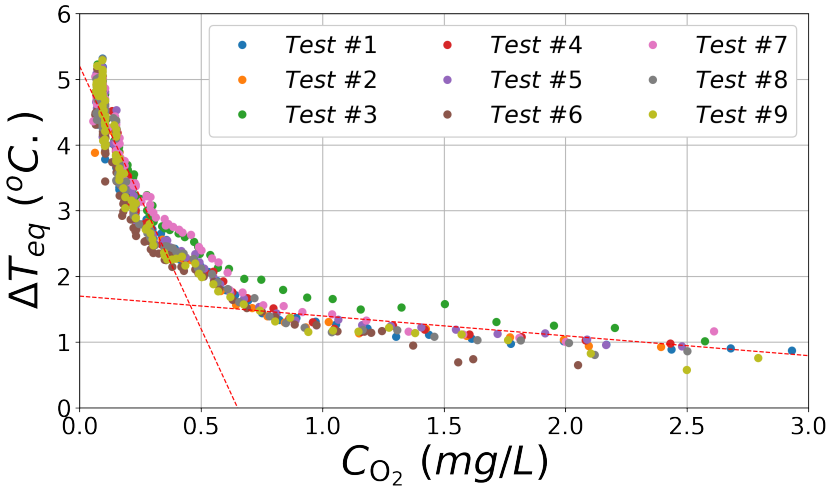

Fig. 14. The correlation between the variables reflecting the liquid degassing and heat-up kinetics C_{O_2} and ΔT_{eq}, found out from the reference test data, was well repeated.

The same exercise is done regarding the already introduced heat and mass transfer rates, respectively denoted as $k_T^L S_i$ and $k_m^L S_i$. The obtained results are presented in Figure 15. In the latter, it appears that the heat transfer rate is the least repeatable during the two-phase regime. However, the asymptotic value of both $k_T^L S_i$ and $k_m^L S_i$ does appear highly repeatable in the studied configuration. At last, 95% of the obtained results stand within a relative uncertainty range of 14%, centered around an average trend, both for the heat and mass transfer rates.

IV. A LUMPED-PARAMETER MODELING OF THE AQUARIUS POOL

Next, a simplified modeling of the phenomenon is introduced with the intent to later simulate the presented reference test (*cf.* Section V). The proposed lumped-parameter model solves the mass and energy balance equations governing the liquid pool volume V_L, depicted in Figure 16. Three so-called conservative variables, whose time-evolution is dictated by these balance equations, are attributed to the control volume: m_L, the liquid mass, m_a^L, the total mass of all gases dissolved

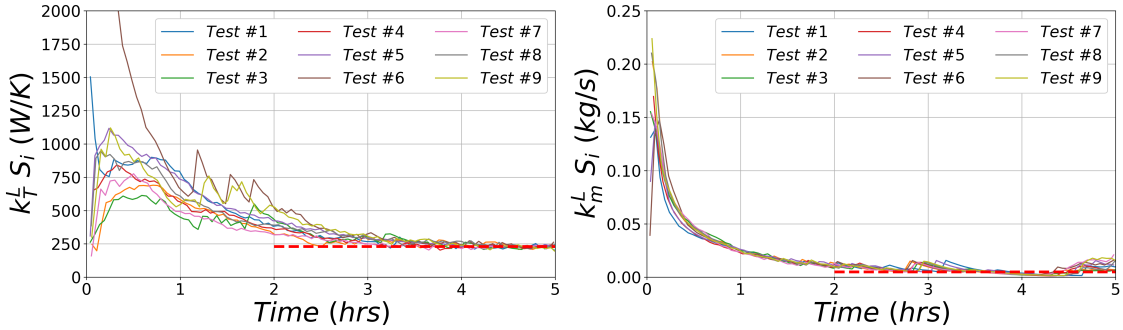

Fig. 15. Repeatability tests. Left: estimate of the gas/liquid heat transfer rate $k_T^L S_i$. Right: estimate of the gas/liquid mass transfer rate $k_m^L S_i$.

in the liquid and U_L, the total internal energy of the liquid. As a modeling assumption, two bounding surfaces allow heat and mass exchanges between the control volume V_L and its surrounding environment. First is the total heaters area, denoted as S_h, which is restricted to heat exchanges. Second is the gas/liquid interfacial area S_i introduced earlier in this article. Across this interface, both heat and mass transfers may develop. Specifically regarding the mass exchanges, both water and dissolved gases may transfer toward the outer environment through the latter. By limiting the exchanges to these two very areas, the heat losses that may develop between the liquid volume V_L and the outer environment are precisely neglected. As seen in [14], those losses are practically negligible for the studied test configurations, thereby justifying their disregard. Further on, the thermal inertia of the heated wall is not modeled and the heated-wall-to-liquid heat transfer is assumed steady at any considered time along the simulations. Then, complying with the specificity of the Aquarius experiments [14], the gas bulk in contact with the liquid volume through the interfacial area S_i is supposed exclusively composed of steam at the temperature $T_{sat}(P_G)$ and pressure P_G. At last, with $k_m^L S_i$ and $k_T^L S_i$, respectively the dissolved gases and heat transfer rates at the gas/liquid interface, the mass and energy balance equations governing the control volume read:

$$\frac{dm_a^L}{dt} = -k_m^L S_i \omega_a^L \tag{13}$$

$$\frac{dm_L}{dt} = \frac{-k_T^L S_i}{\mathcal{L}_w} \left(T_L - T_{sat}(P_G)\right) \tag{14}$$

$$\frac{dU_L}{dt} = \dot{Q}_p - \left|\frac{dm_L}{dt}\right| h_{gsat}(P_G) - P_G \frac{dV_L}{dt} \tag{15}$$

with ω_a^L and $h_{gsat}(P_G)$, respectively the dissolved air mass fraction and the steam saturation specific enthalpy, estimated at pressure P_G.

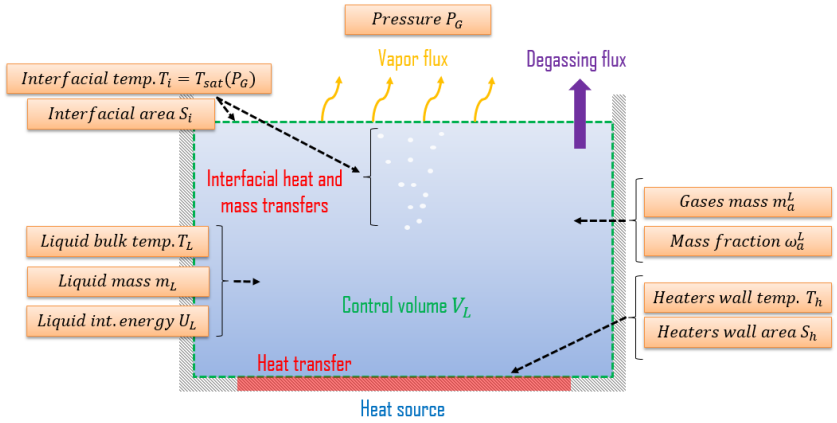

Fig. 16. Illustration of the modeled control volume V_L and its associated conservative and state variables.

In order to be resolved, the above system of equations requires the closure of some of its constitutive variables. First of all are the so-called state variables T_L and ω_a^L. Provided m_L and U_L, one can deduce T_L by first computing the specific liquid internal energy $u_L(T_L, P_G)$ as:

$$u_L(T_L, P_G) = \frac{U_L}{m_L} \tag{16}$$

Then, making use of a thermophysical properties database:

$$u_L(T_L, P_G) \rightarrow T_L \tag{17}$$

Next, ω_a^L is simply approximated by:

$$\omega_a^L \approx \frac{m_a^L}{m_L} \tag{18}$$

provided the dissolved gases are highly diluted in water. Importantly, the control volume V_L is to be calculated. This is done as:

$$V_L = \frac{m_L}{\rho_L(T_L, P_G)} \tag{19}$$

with $\rho_L(T_L, P_G)$ the liquid density, estimated once T_L is known. Further on are the variables involved in the exchanged heat and mass fluxes: $k_m^L S_i$ and $k_T^L S_i$, respectively the already introduced

dissolved gases and heat interfacial transfer rates (*cf.* Section III.B). Those variables are estimated by means of the below set of correlations that was obtained by varying largely the experimental conditions in a regular matrix of 24 tests, as described in [19]. During that experimental campaign, the operating pressure P_G, the initial pool level $z_p(0)$ and the heating power $\dot{Q}_p$ were respectively varied from 22 to 42 mbar, from 20 to 30 cm and from 250 to 1000 W, whereas the initial amount of dissolved oxygen was kept unchanged from one test to another and equal to 6.5 mg/L. Let us detail the obtained correlations. Resulting from an initial search by trial-and-error, a set of four dimensionless numbers has been proven relevant for representing those two-phase heat and mass transfers [19]. First of all is a dimensionless form of the heat transfer rate $k_T^L S_i$, denoted as Φ_T, which reads:

$$\Phi_T = \frac{k_T^L S_i}{(k_T^L S_i)_o} \tag{20}$$

where $(k_T^L S_i)_o$ is an estimated single-phase heat transfer rate, corresponding to the system's temperatures and pressure reached during the two-phase regime and with $S_i = S_p$. The quantity $(k_T^L S_i)_o$ is computed by means of a correlation determined from the single-phase stage of all the considered tests:

$$(k_T^L S_i)_o = 0.6 \times \left(\frac{g\beta_L (T_L - T_{sat}(P_G))\ z_p^3}{\nu_L \kappa_L} \right)^{0.33} \times \frac{\lambda_L\ S_p}{z_p} \tag{21}$$

with g, ν_L and κ_L, respectively the gravitational acceleration, the liquid water kinematic viscosity and thermal diffusivity, λ_L, the liquid water thermal conductivity. In a similar fashion, one can introduce Φ_m, a dimensionless form of the mass transfer rate $k_m^L S_i$, defined as:

$$\Phi_m = \frac{k_m^L S_i}{(k_m^L S_i)_o} \tag{22}$$

where $(k_m^L S_i)_o$ is an estimated single-phase mass transfer rate, corresponding to the system's temperatures, dissolved gases concentration and pressure reached during the two-phase regime and with $S_i = S_p$. The quantity $(k_m^L S_i)_o$ is computed by means of another determined correlation:

$$(k_m^L S_i)_o = 1.6 \times \left(\frac{g\beta_L (T_L - T_{sat}(P_G))\ z_p^3}{\nu_L \kappa_L} \right)^{0.33} \times \frac{\mathcal{D}_{a;w}^L\ S_p}{z_p} \tag{23}$$

with $\mathcal{D}_{a;w}^L$, the dissolved-air/water diffusion coefficient. Next is the so-called Gibbs number, de-

noted as Gb and representing a dimensionless form of the energetic cost ΔF_{max} associated with any bubble nucleation process. This number reads [25]:

$$Gb = \frac{\Delta F_{max}}{k_B T_L} \tag{24}$$

with k_B the so-called Boltzmann's constant and:

$$\Delta F_{max} = \frac{16}{3} \frac{\pi\ \sigma^3}{(P_a^L + P_{sat}(T_L) - P_G)^2} \tag{25}$$

with σ, the water surface tension, P_a^L the partial pressure of air in dissolution within water and $P_{sat}(T_L)$, the water saturation pressure at temperature T_L. Provided ω_a^L and T_L, P_a^L can be estimated by means of the well-known Henry's law, which applies adequately in the present case [26]:

$$P_a^L = \omega_a^L \frac{\mathcal{H}_a(T_L)}{\mathcal{M}_a} \tag{26}$$

with $\mathcal{H}_a(T_L)$, the so-called Henry's constant of dissolved air, evaluated at temperature T_L and $\mathcal{M}_a$ the air molar mass. Then is the well-known Rayleigh number Ra_L, defined as:

$$Ra_L = \frac{g\beta_L \Delta T_L z_p^3}{\nu_L \kappa_L} \tag{27}$$

with:

$$\Delta T_L = T_h - T_{sat}(P_G) \tag{28}$$

and T_h, the measured heaters wall temperature. On that basis, the following two correlations have been derived from the data:

$$\Phi_T = C_T \times Gb^{-0.33} \times Ra_L^{1.5} \tag{29}$$

and

$$\Phi_m = 2\Phi_T \tag{30}$$

where the pre-factor C_T has been proven dependent to the initial pool collapsed level and is fixed to:

- $C_T = 1.86 \times 10^{-11}$ for $z_p(0) = 30$ cm;

- $C_T = 1.15 \times 10^{-10}$ for $z_p(0) = 20$ cm.

Interestingly, those correlations link the transfers intensification that is classically observed under bubbling conditions to the Gibbs number, associated with bubble nucleation processes. According to those correlations, the bigger the energetic cost for bubble nucleation, the lesser the amount of nucleated bubbles and the lesser the intensity of the two-phase heat transfer rate. This interesting finding does appear in complete agreement with the phenomenological observations discussed in Section III.A. Furthermore, the intensification of the two-phase heat and mass transfer rates appears as an increasing function of the intensity of the natural convection flow of the liquid phase, as one might expect. One can notice that for estimating the above Ra_L number, one has to provide a value for the unresolved heated wall temperature T_h (*cf.* Equation (27)). Reminding that the heated-wall-to-liquid heat transfer is assumed steady:

$$T_h = T_L + \frac{\dot{Q}_p}{k_h S_h} \tag{31}$$

with k_h, the heated-wall-to-liquid heat transfer coefficient. Given a correlation for k_h derived from the empirical data and given in [19], this yields:

$$T_h = T_L + \left(\frac{1}{0.23} \frac{\dot{Q}_p}{S_h \lambda_L} \left(\frac{\kappa_L \nu_L}{g \beta_L} \right)^{1/3} \right)^{3/4} \tag{32}$$

with the already introduced liquid bulk parameters κ_L, ν_L, λ_L and β_L estimated by means of a thermophysical properties database, at temperature T_L and pressure P_G.

At last, P_G and $\dot{Q}_p$ are fixed and imposed prior to the solving of the above system of differential equations. Identically, $\mathcal{L}_w(P_G)$, $T_{sat}(P_G)$ and $h_{gsat}(P_G)$ are also constant and given by any thermophysical properties database, once P_G is known. In the below simulation, when needed, all fluid properties were evaluated using the open-source database called *CoolProp* [27]. In the computational program written for simulating the Aquarius experiments, a so-called Euler implicit numerical scheme has been retained and coded. The resolved system of equations is first expressed through a matrix form as follows:

$$\frac{dY}{dt} = F(X, t) \tag{33}$$

with t the time variable, Y the so-called vector of the conservative variables:

$$Y = \begin{bmatrix} m_a^L \\ m_L \\ U_L \end{bmatrix} \tag{34}$$

with X the so-called vector of state variables:

$$X = \begin{bmatrix} \omega_a^L \\ m_L \\ T_L \end{bmatrix} \tag{35}$$

then with F the so-called flux function, returning as a vector form the right-hand-side of the resolved system of equations, provided X and t. The discretization of the above system of equations according to an Euler implicit scheme reads:

$$\frac{Y_{\mathrm{n+1}} - Y_{\mathrm{n}}}{\delta t} = F(X_{\mathrm{n+1}}, t_{\mathrm{n+1}}) \tag{36}$$

with index n attributed to the variables estimated at time t_{n} and index n+1 attributed to the variables estimated at time $t_{\mathrm{n+1}} = t_{\mathrm{n}} + \delta t$. At each time step, knowing X_{n} and Y_{n}, $X_{\mathrm{n+1}}$ and $Y_{\mathrm{n+1}}$ are solved iteratively by a coded Newton-Raphson algorithm. The algorithm convergence is considered if the following condition on Y is fulfilled:

$$\left| \frac{Y^{\mathrm{i+1}} - Y^{\mathrm{i}}}{Y^{\mathrm{i+1}}} \right| \leq \epsilon \tag{37}$$

with i, the iteration index and ϵ, some arbitrary convergence criterion $\ll 1$.

V. THE SIMULATION OF A REFERENCE TEST

In what follows, we finally provide the results of the simulation of the reference test described in Section III, conducted with the proposed lumped-parameter model. The characteristics of the so-called reference test have been already given earlier in this article and are not recalled here. The following numerical settings were retained: time step $\Delta t = 180$ s and precision $\epsilon = 10^{-6}$.

The obtained results are successively presented in the below figures. First of all are depicted, respectively in the left and right-hand sides of Figure 17, the time-trend of the liquid mass m_L and of the liquid vaporization rate $\dot{m}_L$. As one can observe, the simulation reproduces well those two quantities, thereby verifying two important points. On one hand, this good fitting confirms that the heat losses at pool's boundaries, omitted in the lumped-parameter model, are reasonably negligible. On the other hand, the mass and energy balances of the modeled liquid pool are certainly well resolved, since as shown in Section III.A, the liquid steadily vaporizes throughout the test at a rate depending to the first order of the supplied heat power (*cf.* right-hand-side of Figure 5). Next, we compare in Figure 18 the simulated liquid thermal metastability degree ΔT_{eq} with the one estimated from the reference test data. It is to be noted that the overall trend of this very variable is well reproduced, with however some apparent slight delay, of the order of 30 min. The actual asymptotic value of ΔT_{eq}, denoted as $\Delta T_{eq;\infty}$, is almost reached by the simulation, with a discrepancy of the order of 0.5°C. As it has been discussed earlier in this paper, the instant amount of dissolved gases contained in the liquid pool is another important variable for describing the phenomenon. Its related counterparts, *i.e.* the dissolved O_2 mass concentration C_{O_2} and degassing rate $\dot{C}_{O_2}$, are both plotted in Figure 19. Overall, one can notice that the trend of the latter two variables is well reproduced by the lumped-parameter model. But, as for the thermal metastability degree depicted in Figure 18, there exists some time lag between the simulated and actual oxygen degassing variables, which is of the order of 30 min too. Obviously, this lag leads to some noticeable discrepancy in the simulated and actual maximum values of $\dot{C}_{O_2}$, as seen in the right-hand-side graph of Figure 19. Further on, the simulated interfacial heat and mass transfer rates, denoted as $k_T^L S_i$ and $k_m^L S_i$, exhibit a similar trend with an appreciable discrepancy at the beginning of the reference test (Figure 20). At last, when combining both ΔT_{eq} and C_{O_2} in Figure 21, it can be observed that the correlation between the instant liquid thermal metastability degree and dissolved O_2 mass concentration is fairly well reproduced, with the same doubly-linear trend. This result may seem surprising at first glance, on the basis of the time lags that have been highlighted above. But, these time lags being of the same order of magnitude for both ΔT_{eq} and C_{O_2}, it is not counter-intuitive to observe nevertheless the same correlation between these variables. Overall, having those first results in mind, one can argue that the proposed lumped-parameter model of the Aquarius pool is able to simulate the reference test with moderate

discrepancies. Nevertheless, the latter might motivate some improvements in the utilized heat and mass transfer correlations for the two-phase regime, which constitutes a perspective of the present work.

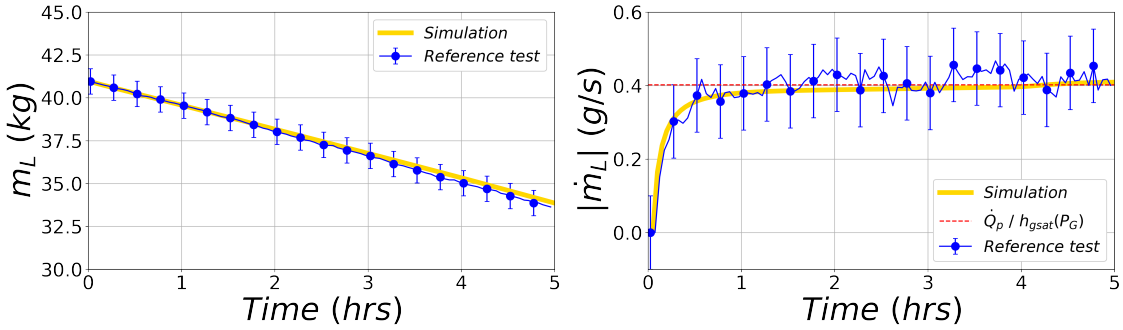

Fig. 17. Simulation of the reference test. Left: liquid mass m_L. Right: liquid vaporization rate $\dot{m}_L$.

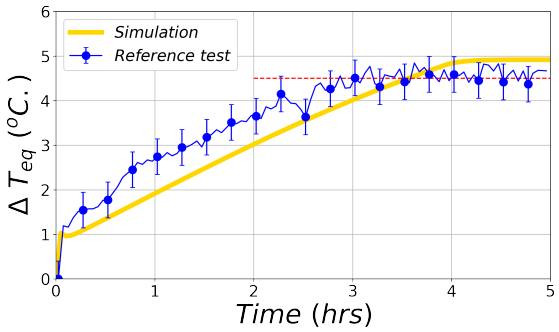

Fig. 18. Simulation of the reference test. Time-trend of the thermal metastability degree of the heated liquid ΔT_{eq}.

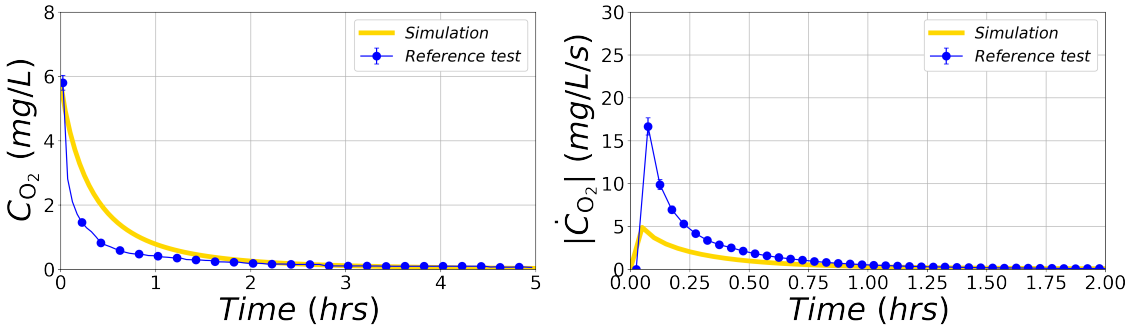

Fig. 19. Simulation of the reference test. Left: dissolved oxygen mass concentration C_{O_2}. Right: oxygen degassing rate $\dot{C}_{O_2}$.

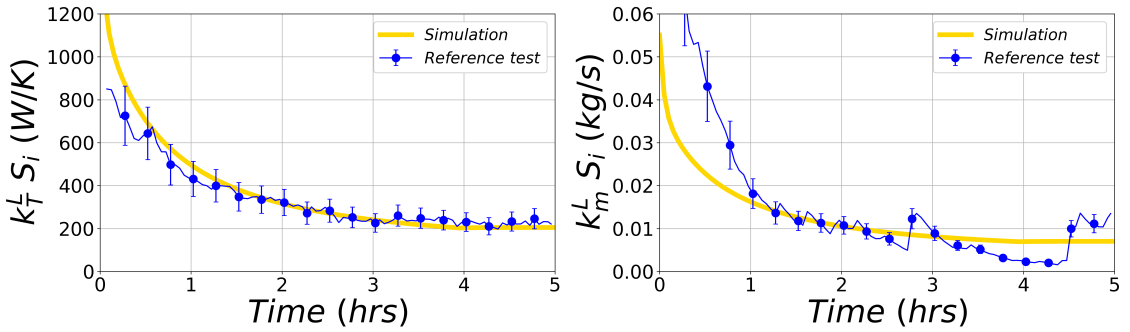

Fig. 20. Simulation of the reference test. Left: interfacial heat transfer rate $k_T^L S_i$. Right: interfacial mass transfer rate $k_m^L S_i$. The unresolved initial value of those transfer rates is intentionally fixed to zero.

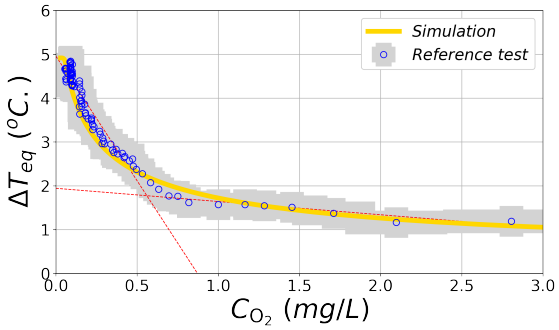

Fig. 21. Simulation of the reference test. Correlation between the variables reflecting the liquid degassing and heat-up kinetics, C_{O_2} and ΔT_{eq}.

VI. CONCLUSION

In this article, an overview of the empirical observations related to the gravity-driven flashing of metastable water in pools heated from below, achieved to date by means of the Aquarius test device, has been first provided. These novel results are indeed of interest for a better understanding of the thermal-hydraulics of SFPs under loss-of-cooling accident conditions. Next, a set of heat and mass transfer correlations has been derived from the data series of each test composing a so-called regular experimental matrix. The correlations that have been found for the two-phase regime are rather original in their mathematical formulation. Interestingly, those correlations link the transfers intensification that is classically observed under bubbling conditions to the Gibbs number, associated with bubble nucleation processes. According to those correlations, the bigger the energetic cost for bubble nucleation, the lesser the amount of nucleated bubbles and the lesser the intensity of the two-phase heat transfer rate. This interesting finding does appear in complete agreement with the phenomenological observations discussed in this article. Furthermore, the intensification of the two-phase heat and mass transfer rates has appeared as an increasing function of the intensity of the natural convection flow of the liquid phase, as one might expect. Another interesting point is the highlighted dependency between the pre-factor of those correlations and the initial water level, imposed prior to any test. Finally, a lumped-parameter modeling of the Aquarius pool, taking benefit from the obtained transfer correlations, has been proposed. The model describes the mass and energy balance equations governing the liquid pool volume. Three so-called conservative variables, whose time-evolution is dictated by these balance equations, are attributed to the liquid pool control volume: the liquid mass, the total mass of all gases dissolved in the liquid and the total internal energy of the liquid. Later on, the model has been successfully compared with the empirical data of a reference test, with moderate discrepancies that could be further reduced as a perspective of the present work.

For that purpose, a better characterization of the heat and mass transfer correlations that have been defined during the present research appears unavoidable. First of all, the single-phase mass transfer correlation describing the air degassing process needs to be improved, taking benefit from more precise measurements when the gas depletion is almost complete (*i.e.* by using a dissolved O_2 optical sensor of better accuracy within the targeted range of small O_2 concentrations). Next, the highlighted variations of the pre-factor of the obtained two-phase heat and mass transfer

correlations are to be better understood by means of more tests, started with a wider range of initial pool levels. Eventually, this work would allow the definition of another correlation, linking the above pre-factor to the initial value of the pool level. Another interesting perspective would be to use the introduced lumped-paramter model, once improved on the basis of the previous suggestions, for predicting the gravity-driven flashing of superheated water within a real, full-scale SFP, under loss-of-cooling accident conditions.

REFERENCES

[1] OECD/NEA, "Status report on spent Fuel Pools under Loss-of-Cooling and Loss-of-Coolant Accident Conditions," , OECD/NEA (2014).

[2] OECD/NEA, "Phenomena Identification and Ranking Table : R&D Priorities for Loss-of-Cooling and Loss-of-Coolant Accidents in Spent Nuclear Fuel Pools," , OECD/NEA (2018).

[3] J. Martin and N. Trégourès, "OECD/NEA R&D priorities for loss-of-cooling and loss-of-coolant accidents in Spent-Fuel-Pools," *Nuclear Engineering and Design*, **410**, 112380 (2023).

[4] Y. Liao and D. Lucas, "Computational modeling of flash boiling flows: A literature survey," *International Journal of Heat and Mass Transfer*, **111**, 246 (2017).

[5] P. Debenedetti, *Metastable Liquids: Concepts and Principles*, Princeton University Press (1996).

[6] J. M. Delhaye, M. Giot, and M. L. Riethmuller, *Thermohydraulics of two-phase systems for industrial design and nuclear engineering*, McGraw-Hill Book Company (1981).

[7] H. M. Kottowski-Dümenil, *Liquid metal thermal-hydraulics*, Inforum Verlag (1994).

[8] K. Mørch, "Reflections on cavitation nuclei in water," *Physics of Fluids*, **19**, 072104 (2007).

[9] A. L. Manera et al., "Stability of natural-circulation-cooled boiling water reactors during startup: experimental results," *Nuclear Technology*, **143**, 77 (2003).

[10] M. Furuya et al., "Flashing-induced density wave oscillations in a natural circulation BWR - mechanisms of instability and stability map," *Nuclear Engineering and Design*, **235**, 1557 (2005).

[11] D. Saury, S. Harmand, and M. Siroux, "Flash evaporation from a water pool: Influence of the liquid height and of the depressurization rate," *International Journal of Thermal Sciences*, **44**, 953 (2005).

[12] S. Gopalakrishna, V. M. Purushothaman, and N. Lior, "An experimental study of flash evaporation from liquid pools," *Desalination*, **65**, 139 (1987).

[13] J. I. Kim and N. Lior, "Some critical transitions in pool flash evaporation," *International Journal of Heat and Mass Transfer*, **40**, 2363 (1997).

[14] J. Martin, P. Ruyer, M. Duponcheel, and Y. Bartosiewicz, "An experimental study of the gravity-driven flashing of metastable water in a pool heated from below," *19th NURETH conference*, Brussels, Belgium, March 6-11, ANS (2021).

[15] A. Wassel, A. Mills, D. Bugby, and R. Oehlberg, "Analysis of radionuclide retention in water pools," *Nuclear Engineering and Design*, **90**, 87 (1985).

[16] J. Martin, G. Brillant, C. Duriez, N. Trégourès, and C. Marquié, "The IRSN DENOPI project: a research program on spent-fuel-pool loss-of-cooling and loss-of-coolant accidents," *Proc. 17th NURETH conference*, Xi'an, Shaanxi, China, Sept. 3-8, ANS (2017).

[17] B. Migot and J. Martin, "An experimental study of the thermal-hydraulics of a spent nuclear fuel pool under loss-of-cooling accident conditions. Part I: the MIDI facility and its main experimental results," *Nuclear Engineering and Design*, **426**, 113404 (2024).

[18] J. Martin and B. Migot, "An experimental study of the thermal-hydraulics of a spent nuclear fuel pool under loss-of-cooling accident conditions. Part II: a first interpretation of the MIDI tests," *Nuclear Engineering and Design*, **426**, 113406 (2024).

[19] J. Martin, "The gravity-driven flashing of metastable water in a pool heated from below - An experimental study," PhD Thesis, Université Catholique de Louvain (Louvain-la-Neuve - Belgique) (2023).

[20] J. Martin, P. Ruyer, M. Duponcheel, and Y. Bartosiewicz, "The role played by dissolved gases during the gravity-driven flashing of superheated water in a spent fuel pool under loss of cooling conditions," *13th NUTHOS conference*, Taichung, Taiwan, September 5-10, ANS (2022).

[21] J. Martin, P. Ruyer, M. Duponcheel, and Y. Bartosiewicz, "A novel experimental observation of the gravity-driven flashing of metastable water in a heated pool," *Nuclear Engineering and Design*, **410**, 112371 (2023).

[22] JCGM, "Guide to the expression of uncertainty in measurement," JCGM 100:2008, JCGM (2008).

[23] E. Cussler, *Diffusion - Third Edition*, Cambridge University Press (2009).

[24] P. Papon and J. Leblond, *Thermodynamique des états de la matière*, Hermann (1990).

[25] C. Brennen, *Cavitation and bubble dynamics*, Cambridge University Press (2014).

[26] D. Green and M. Southard, *Perry's Chemical Engineers' Handbook - 9^{th} Edition*, MacGraw-Hill (2018).

[27] I. H. Bell, J. Wronski, S. Quoilin, and V. Lemort, "Pure and pseudo pure fluid thermophysical property evaluation and the open-source thermophysical property library CoolProp," *Industrial and Engineering Chemistry Research*, **53**, 2498 (2014).